Electronic Supplementary Material (ESI) for Materials Horizons.

Electronic Supplementary Information for "*Colloidal nano-toolbox for molecularly regulated polymerization: chemorheology over 6 decades of viscoelasticity*"

Amir Sheikhi,[1*+] Han Yang,[1] Pierre J. Carreau,[2] Theo G.M. van de Ven[1*]

[1]Department of Chemistry, Quebec Centre for Advanced Materials (QCAM), Pulp and Paper Research Centre, McGill University, Montreal, 3420 University Street, QC, H3A 2A7, Canada.

[2]Research Centre for High Performance Polymer and Composite Systems (CREPEC), Chemical Engineering Department, École Polytechnique de Montréal, PO Box 6079, Stn Centre-Ville, Montreal, QC, H3C 3A7, Canada.

The Electronic Supplementary Information (ESI) includes Materials and Methods, two Tables, rheology data (15 Figures), and the mechanism of rheology modification using nanocelluloses (one Scheme).

---

[*] Corresponding authors: amir.sheikhi@mail.mcgill.ca, and theo.vandeven@mcgill.ca
[+] Current address: Biomaterials Innovation Research Center, Harvard-MIT Division of Health Sciences and Technology, Massachusetts Institute of Technology (sheikhi@mit.edu), and Harvard Medical School (asheikhi@bwh.harvard.edu), MA 02139, USA.

Materials and Methods

The cellulose-based nano-toolbox used for engineering the macromolecular interactions of AZC is illustrated in Scheme 1 and presented in Table S1.

Table S1. Nanocellulose toolbox for tuning macromolecular interactions in dynamic, network-forming systems.

Nanocellulose	Surface functionality	Hydrodynamic/TEM size (length×width, nm)	Notes
CNC	$-SO_3^-$, ~ 0.3 mmol g^{-1}	50/100×5[1,2]	
TEMPO-CNC	$-SO_3^-$, ~ 0.3 mmol g^{-1} $-COO^-$, ~ 0.5 mmol g^{-1}	50/100×5	
ENCC	$-COO^-$, ~ 5.2 mmol g^{-1}	220/100×5[1–4]	
HENCC-1	$-COO^-$, ~ 2 mmol g^{-1}	150/100×5[3]	Hydrolyzed for 3 h
HENCC-2	$-COO^-$, ~ 0.34 mmol g^{-1}	-	Hydrolyzed for 16 h
DCC*	$-COO^-$, ~ 5.8 mmol g^{-1}	150/-	
SNCC	-COH, ~ 6 mmol g^{-1}	190/100×5[2,3]	
CNF	$-COO^-$, ~ 0.65 mmol g^{-1}	-/550×5[5]	
CNFOH	$-CO-NH-CH_2-CH_2-OH$, ~ 0.3 mmol g^{-1} $-COO^-$, ~ 0.3 mmol g^{-1}	-/550×5	

*note: DCC is not a nanocellulose, but a water-soluble cellulosic polyelectrolyte. It is included in the list, because the protruding chains in ENCC (the "hairs") have the same chemical composition as DCC.

Materials

Q-90 softwood kraft pulp sheets and conventional cellulose nanocrystal (CNC) powder (prepared by sulfuric acid treatment) were provided by FPInnovations (Montreal, Canada) and cellulose nanofibrils (CNFs) were obtained from Forest Products Laboratory (Madison, WI, USA). Sodium (meta)periodate (≥ 99 %), ethylene glycol (≥ 99 %), hydroxylamine hydrochloride (≥ 99 %), sodium chlorite (80 %), sodium bicarbonate (99.5-100.5 %), methanol (99.8 %), ethanolamine (≥ 98 %), 4-(4,6-dimethoxy-1,3,5-triazin-2-yl)-4-methylmorpholinium chloride (DMTMM, ≥ 96 %), and ammonium zirconium carbonate (50 %, 1-2 % tartaric acid as stabilizer) were purchased form Sigma-Aldrich. Hydrogen peroxide (30 %) was supplied by Fisher. Hydrogen chloride (0.1 M and 1 M) and sodium hydroxide (10 mM, 0.1 M, and 1 M) were purchased from Fluka. Anhydrous ethyl alcohol was purchased from Commercial Alcohols. Sodium chloride was supplied by ACP Chemicals Inc. All chemicals were used as received. Milli-Q water (18.2 MΩ cm, Millipore Milli-Q Purification System) was used in all experiments.

Methods

Preparation of CNC, ENCC, DCC, HENCC, and SNCC[2,3,6–9]

CNC dispersions were prepared by overnight stirring the spray-dried CNC in DI water. ENCC was produced according to a previously published method. Briefly, pre-soaked softwood pulp was first oxidized by periodate for 96 h (1 g of pulp and 1.33 g of $NaIO_4$ were mixed with 66 mL of water in a beaker, which was wrapped with aluminum foil to prevent light exposure and periodate deactivation), followed by overnight oxidation using sodium chlorite (1.41 g of

$NaClO_2$, 1.41 g of H_2O_2, 2.93 g of NaCl, and 50 mL of water were used for 1 g of periodate oxidized pulp) at constant pH = 5, maintained by gradually adding 0.5 M NaOH. ENCC was separated from the suspension of two-step oxidized cellulose by the addition of ethanol followed by centrifugation (5000 rpm for 10 min, Beckman Coulter J2 centrifuge and JA-25.50 fixed angle rotor). DCC was isolated from the supernatant after the separation of ENCC by further addition of ethanol, followed by centrifugation (5000 rpm for 10 min). HENCC was prepared by the hydrolysis of ENCC with 3 N HCl at 45°C for a desired time, shown in **Table 1**. The excess HCl was neutralized by adding $NaHCO_3$ to stop the hydrolysis reaction. Finally, the HENCC suspensions were purified by dialysis (MWCO = 12-14 kDa) against DI water. SNCC was synthesized by heating the periodate oxidized cellulose at 80°C in a round bottom flask: one gram periodate-oxidized cellulose pulp was suspended in 100 g water including the moisture in the pulp, followed by heating and gentle stirring for 6 h. The suspension was centrifuged to remove the non-fibrillated fibers (15000 rpm for 10 min), and subsequently, SNCC was separated by the addition of propanol to the supernatant followed by centrifugation (5000 rpm for 10 min).

Preparation of TEMPO-CNC

TEMPO-oxidized CNC (TEMPO-CNC) was prepared by reacting 1 g of CNC with 0.8 mg of 2,2,6,6-tetramethylpiperidinyl-1-oxyl (TEMPO), 0.56 g of $NaClO_2$, and 100 mL of phosphate buffer (pH 6.8) in a three-neck round-bottom flask, stirred at 500 rpm. Then, 0.125 mL of NaClO was added to the flask when the temperature reached 50°C. The reaction was maintained at 60 °C for 24 hours, and the suspension was precipitated by adding ethanol, followed by washing with a water-ethanol solution and purifying through dialysis against DI water.

Preparation of CNFOH

The conjugation of CNF with amidoethanol was performed as follows: ethanolamine (molar mass was four times as carboxyl group content of CNF) was added to the CNF suspension and mixed by stirring for half an hour. DMTMM (molar mass was the same as carboxyl groups content of CNF) was first dissolved in 3 mL water and then added dropwise to the ENCC suspension. The reaction was continued for overnight. The CNF suspension was then purified by dialysis (12-14 kDa) for 2 days.

Charge density measurement by conductometric titration

Conductometric titration was performed to obtain the charge density of ENCC, HENCC, CNF, and CNC before and after chemical modifications using a Metrohm 836 Titrando titrator. Typically, a sample including 0.02 g of solid and 2 mL of 20 mM NaCl was added to 140 mL of Milli-Q water. Starting from pH ~ 3.2, 10 mM NaOH solution was added at 0.1 mL min^{-1} to the suspension to reach pH ~ 11. The carboxylic acid content of each sample was calculated based on the weak acid region in the titration curve.[10]

Rheology

The dynamic evolution of nanocomposite viscoelastic properties (storage *G'* and loss *G''* moduli) was registered with time upon heating at 80°C through small-amplitude oscillatory shear (SAOS) rheology using a stress-controlled rheometer (Physica MCR 501, Anton Paar) equipped with a cone-and-plate geometry (radius ~ 25 mm and cone angle ~ 0.04 rad, sample volume ~ 3.5 mL).

For each experiment, ~ 3.5 mL sample was placed in a single cuvette holder at room temperature followed by heating to 80°C within exactly 5 min (heating rate = 11.4°C min^{-1}). Thereafter, time sweep, frequency sweep, and linear viscoelasticity (LVE) tests were conducted. Each time sweep was performed at constant strain (γ = 5 %) and frequency (ω = 0.5 rad s^{-1}) for ~ 5.5 h. The frequency sweep was conducted immediately after the time sweep at $\omega = 0.01\text{-}10$ rad s^{-1} and a constant strain ($\gamma = 5$ %). Two LVE tests at $\omega = 0.1$ rad s^{-1} and 10 rad s^{-1} and $\gamma = 1\text{-}10$ %, respectively, guaranteed the linearity of viscoelastic moduli.

Rheology data

ENCC/DCC nanocomposites

Figure S1 presents the storage and loss moduli of ENCC/DCC nanocomposites. The AZC (0.5 %) solution (black), in the absence of any additive, undergoes time-dependent crosslinking, manifested in the increase in storage modulus (*G'*) while also becoming more viscous, as suggested by the loss modulus (*G''*) elevation. The dynamics of AZC crosslinking comprise an induction time (t_i ~ 1000 s) during which the crosslinking takes place slowly. During the induction time, the network formation rate increases to reach the most rapid dynamics of the whole crosslinking process at t_i. Thereafter, while *G'* and *G''* increase, their rate decreases to result *G'* ~ 30 Pa and *G''* ~ 0.6 Pa at *t* ~ 5.5 h. This process is solely controlled by the self-crosslinking of AZC molecules, which depends on the AZC concentration, temperature, and incubation time. These parameters are maintained constant in all our experiments.

When 0.1 % ENCC is added to AZC, surprisingly, the final storage modulus (after 5.5 h) is tremendously decreased to *G'* ~ 0.55 Pa (~ 60 times decrease as compared to AZC). In addition, such decrease is more pronounced using DCC (light blue symbols), which results in *G'* ~ 0.003 Pa, i.e., ~10^5 times reduction. Given that the high carboxyl group content of ENCC (~ 5.2 mmol g^{-1}) and DCC (~ 5.8 mmol g^{-1}) promotes bond formation with AZC, the decrease in *G'* suggests that hydrogen bonding is not the only governing mechanism in this composite gel. Interestingly, by an increase in the ENCC concentration to 0.5 % (green symbols), the viscoelastic moduli further decrease.

Carboxyl groups on ENCC/DCC form hydrogen bonds with AZC molecules, which results in the adsorption of single or self-crosslinked AZC molecules on ENCC/DCC. While part of the AZC molecules undergo self-crosslinking, they attach to the nanocelluloses and remain separated from each other due to the strong colloidal repulsion among ENCC/DCC. The effective length scale of electrostatic repulsive forces is tens of nanometers (depending on the ionic strength); whereas hydrogen bonding is effective within *O*(Å) lengths.

To examine our hypothesis, we decreased the electrostatic forces by shrinking the diffuse layer around the nanocelluloses using KCl salt (0.5 M, orange symbols). While *G'* of a salt-free AZC-ENCC system ~ 0.55 Pa, that of a salty system ~ 3.5 Pa. Such a 6-fold increase in *G*' attests that reducing the repulsion between the colloidal particles results in a stronger network. Note that, increasing the salt concentration to achieve better crosslinking does not seem to be industrially feasible, because it decreases the maximum crosslinking efficiency by a factor of ~ 6 (as suggested by comparing the salt-free AZC system, black symbols, and salty AZC system, red symbols, in Figure S1).

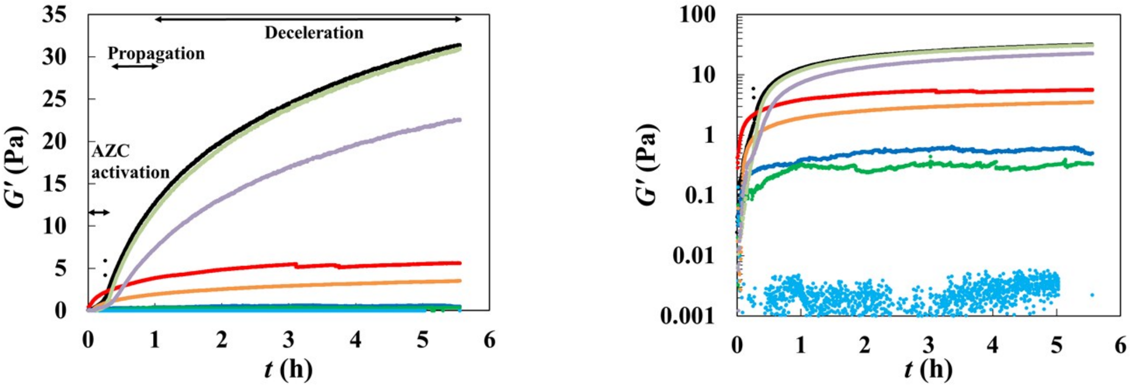

(a) Storage modulus *G'* versus time *t* (left: regular, right: semi-logarithmic scales) at $\omega = 0.5$ rad s^{-1}.

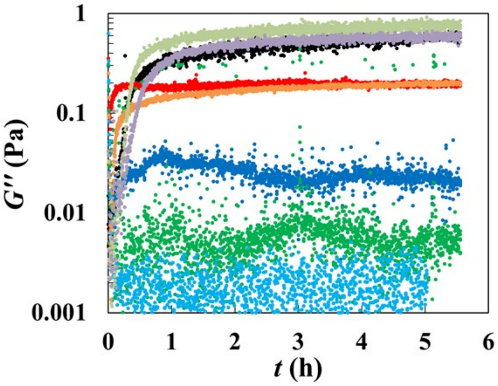

(b) Loss modulus *G''* versus time *t* at $\omega = 0.5$ rad s^{-1}.

Fig. S1: Viscoelastic evolution of AZC (0.5 %)-ENCC/DCC nanocomposites at 80°C. Color legend is as follows: black (no additive), red (KCl 0.5 M), orange (ENCC 0.1 %, KCl 0.5 M), light green (ENCC 0.001 %), purple (ENCC 0.01 %), dark blue (ENCC 0.1 %), green (ENCC 0.5 %), and light blue (DCC 0.1 %).

Besides the absolute value of viscoelastic moduli, the time required to reach a desired heat-sensitive hydrogel is of utmost industrial importance. Therefore, the rate of storage and loss moduli change is calculated by considering a 200 s time window. For all nanocomposites, the nanoparticle/biopolymer significantly decreases the rate of gel formation. The rate is similarly correlated to the repulsion forces among the nanospecies: the higher the repulsion, the lower the gel formation rate.

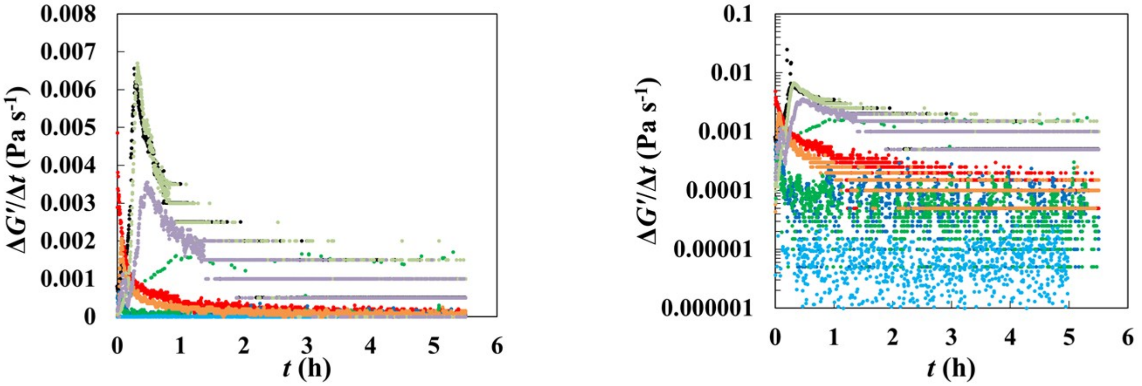

Fig. S2: Rate of storage modulus evolution versus time for ENCC/DCC nanocomposites at 80°C and $\omega = 0.5$ rad s^{-1}, in (left) regular and (right) semi-logarithmic scales. The color legend is the same as **Fig. S1**. Note that $\Delta t = 200$ s.

Industrial material processes usually induce different types of stress to the material, namely, tensile, compressive, and shear. The viscoelastic behavior of ENCC/DCC nanocomposites upon applying shear stress was investigated. **Figure S3** shows the storage and loss moduli of the nanocomposites upon sweeping the frequency in the range of 0.01-10 rad s^{-1}. It is evident from the right panel that these materials are all shear-thinning, i.e., the real part of the complex viscosity $\eta' = G''/\omega$ decreases by increasing ω.

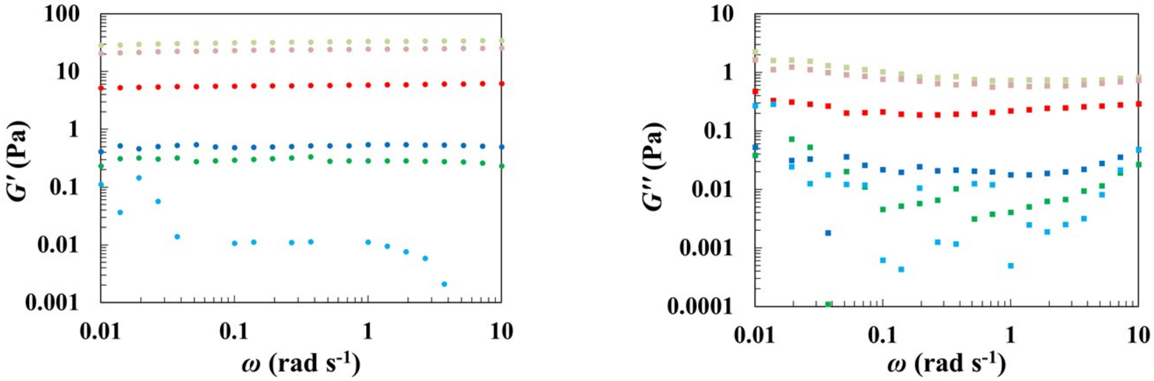

Fig. S3: Storage (left) and loss (right) moduli dependency of ENCC/DCC nanocomposites on frequency, after gel formation at 80°C for 5.5 h. Color legend is the same as **Fig. S1**.

HENCC nanocomposites

The goal of this section is to systematically decrease the ENCC charge content (to possibly decrease the electrosteric repulsion and increase the network strength). **Figure S4** presents the storage and loss moduli for AZC-HENCC nanocomposites bearing different carboxyl group contents. Compared to the AZC (0.5 %, black symbols) system, at a high surface charge content (2 mmol g^{-1}), a high particle concentration (0.5 %, dark blue symbols in **Fig. S4**) results in the lowest *G'* and *G''* due to a high AZC adsorption capacity along with a strong interparticle repulsion. It is noteworthy that, expected from our hypothesis, *G'* and *G''* of HENCC are still larger than ENCC nanocomposites. Decreasing the particle concentration and/or charge, results in further increase in *G'* and *G''*. Interestingly, opposite to all cases with decelerated gel formation dynamics, when the particle charge is low (0.34 mmol g^{-1}) and its concentration is high (0.5 %, green symbols, **Fig. S4**), the loss and storage moduli keep increasing almost linearly. Although these particles increase the induction time, the linear gel formation dynamics provides higher *G'* and *G''* than other cases at high enough time spans. Accordingly, depending on the industrial processing time (e.g., extrusion residence time), such nanocomposites may help improve the properties of AZC-mediated crosslinking.

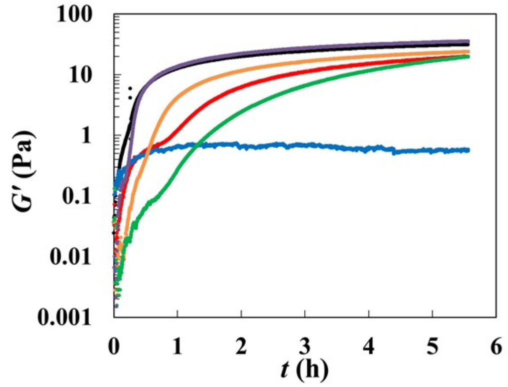

(a) Storage modulus *G'* versus time *t* at $\omega = 0.5$ rad s^{-1}.

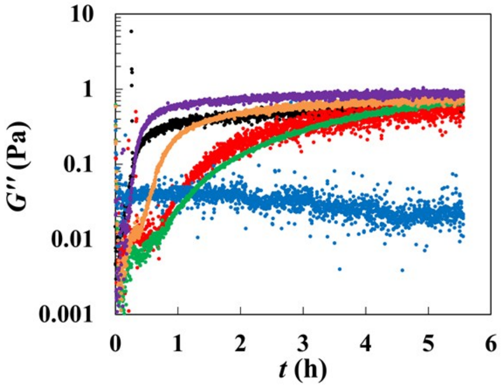

(b) Loss modulus *G''* versus time *t* at $\omega = 0.5$ rad s^{-1}.

Fig. S4: Viscoelastic evolution of AZC (0.5 %)-HENCC nanocomposites at 80°C. Color legend is as follows: black (no additive), orange (HENCC 0.34 mmol g^{-1}, 0.1 %), red (HENCC 2 mmol g^{-1}, 0.1 %), green (HENCC 0.34 mmol g^{-1}, 0.5 %), dark blue (HENCC 2 mmol g^{-1}, 0.5 %), purple (HENCC 2 mmol g^{-1}, 0.01 %).

The maximum gel formation rate, shown in **Fig. S5**, is higher and is obtained faster for lower surface charge and/or nanocellulose concentrations. Moreover, at a certain time and particle concentration, the rate is lower for higher surface charges, up to $t \sim 2.8$ h after which it remains constant when the particle charge is low (e.g., 0.34 mmol g^{-1}) and its concentration is high (green symbols, averaged by black line), while for other cases, it keeps decreasing.

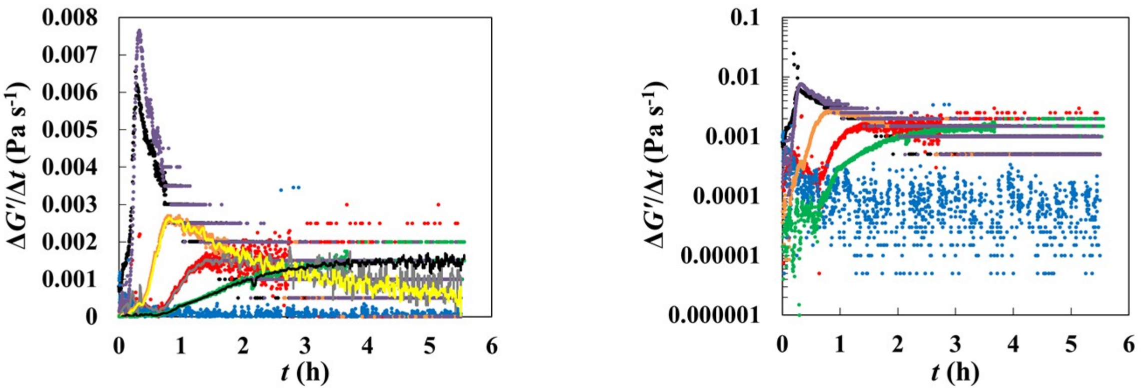

Fig. S5: Rate of storage modulus evolution versus time for HENCC nanocomposites at 80°C and $\omega = 0.5$ rad s^{-1}, (left) regular and (right) semi-logarithmic scales. The color legend is the same as **Fig. S4**. Note that $\Delta t = 200$ s. In the left panel, the lines show average values to highlight the trends.

Fig. S6 presents the storage and loss moduli dependency on the oscillatory frequency. Similar to the ENCC/DCC nanocomposites, dispersing HENCC in AZC solutions results in shear-thinning hydrogels.

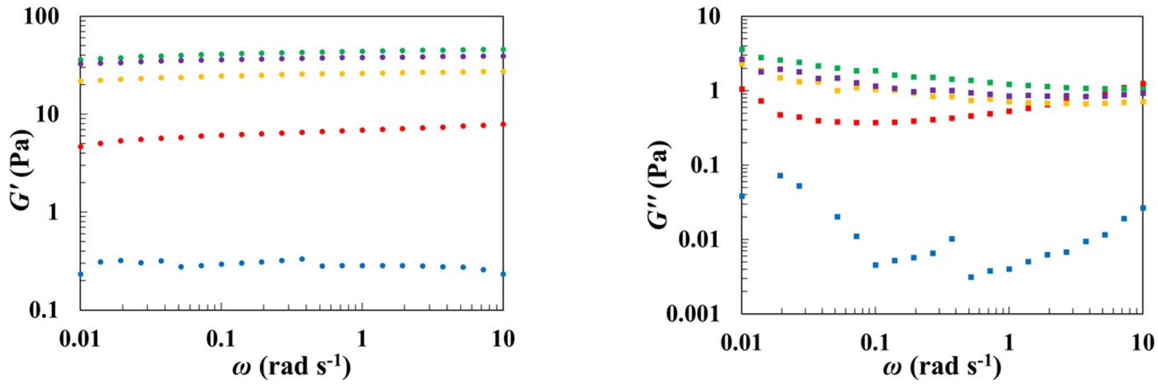

Fig. S6: Storage (left) and loss (right) moduli dependency of HENCC nanocomposites on frequency, after gel formation at 80°C for 5.5 h. Color legend is the same as **Fig. S5**. Note that the green symbols (HENCC, 0.34 mmol g^{-1}, 0.1 %) represent the frequency sweep after ~ 1 h. Shear thinning behavior of all samples is evident.

CNC nanocomposites

CNC has the same crystalline body as ENCC/HENCC while bearing hydroxyl and sulfate half ester groups instead of carboxyl groups; therefore, it is significantly less charged than ENCC/HENCC. In addition, it does not accommodate any amorphous region. **Figure S7** presents the viscoelastic properties of CNC nanocomposites versus time at 80°C. While a low CNC concentration (0.1 %) has no significant effect on the viscoelastic properties (compare black and red colors in **Fig. S7**), increasing the CNC content to 0.5 %, increases *G'* and *G''* by a factor of ~ 2 and ~ 4, respectively. The surface charge of CNC is significantly lower than ENCC (more than 10 times); therefore, the repulsion among nanoparticles is less pronounced. Once the AZC molecules attach to CNC, further CNC-AZC-CNC conjugation becomes possible. In such condition, viscoelasticity can be improved by increasing the CNC concentration.

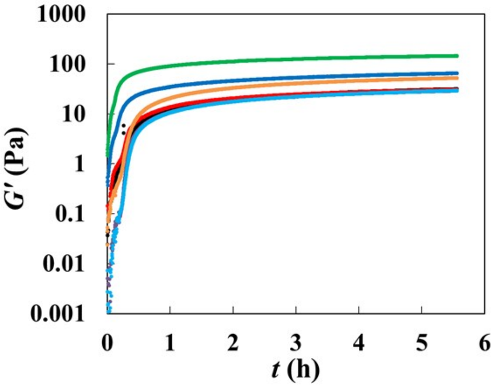

(a) Storage modulus *G'* versus time *t* at $\omega = 0.5$ rad s^{-1}.

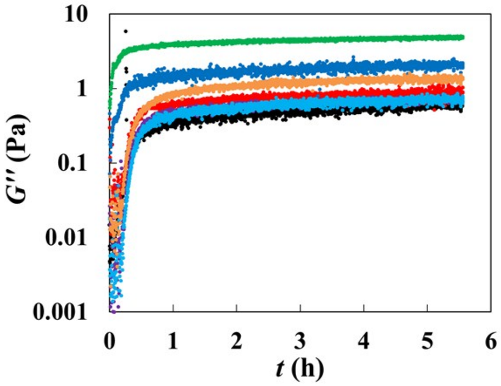

(b) Loss modulus *G''* versus time *t* at $\omega = 0.5$ rad s^{-1}.

Fig. S7: Viscoelastic evolution of AZC (0.5 %)-CNC nanocomposites at 80°C. Color legend is as follows: black (no additive), red (CNC 0.1 %), dark blue (CNC 0.5 %), green (CNC 1 %), orange (TEMPO-CNC 0.5 %), light blue (TEMPO-CNC 0.1 %), purple (TEMPO-CNC 0.01 %).

The crosslinking rate is shown in **Fig. S8**. This figure attests that embedding CNC in AZC metallogels results in a faster crosslinking than a CNC-free system.

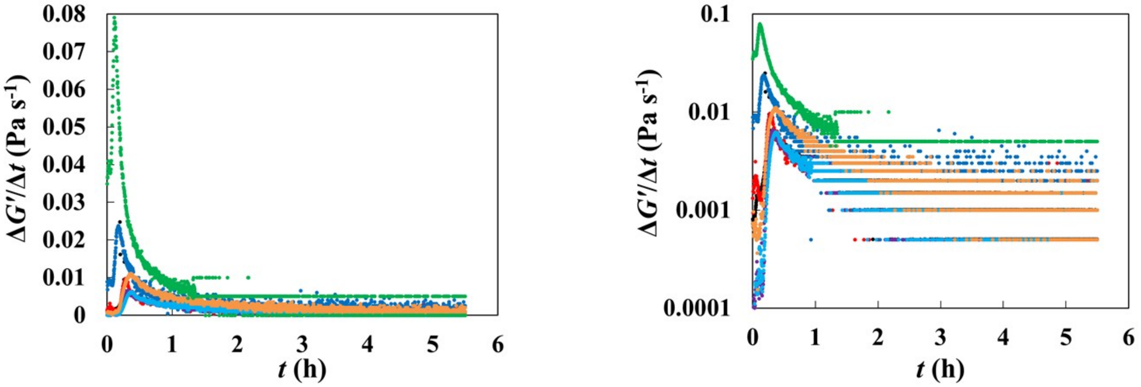

Fig. S8: Rate of storage modulus evolution versus time for CNC nanocomposites at 80°C and $\omega = 0.5$ rad s^{-1}, (left) regular and (right) semi-logarithmic scales. The color legend is the same as **Fig. S7**. Note that $\Delta t = 200$ s.

Frequency sweep of these nanocomposites (**Fig. S9**) indicates a shear-thinning behavior.

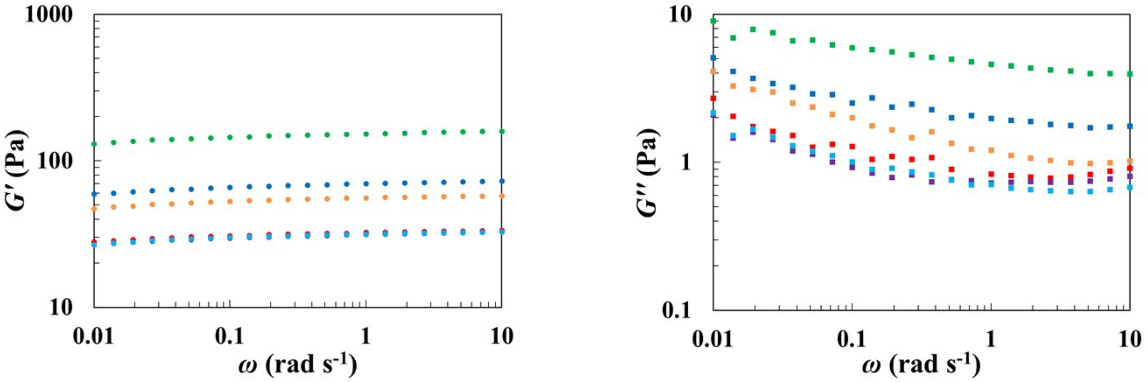

Fig. S9: Storage (left) and loss (right) moduli dependency of CNC nanocomposites on frequency, after gel formation at 80°C for 5.5 h. Color legend is the same as **Fig. S7**. All samples have shear thinning behavior.

CNF nanocomposites

CNFs are uncooked spaghetti-like nanofibers with a width similar to CNC and ENCC. The carboxyl content is ~ 0.65 mmol g^{-1}, and they bear hydroxyl groups similar to CNC and ENCC. **Figure S10** presents the storage and loss moduli of different types of AZC-CNF nanocomposites. Adding 0.1 % CNF to AZC (red symbols, **Fig. S10**), initially accelerates the *G'* and *G''*; whereas, the final values of viscoelastic properties remain comparable to the CNF-free AZC (black symbols). Increasing the CNF concentration to ~ 0.5 %, increases *G'* and *G''* by a factor of ~ 4 and ~ 2, respectively, which are both very similar to the CNC nanocomposites.

While 0.1 % CNF or CNC does not have any significant effect on the viscoelasticity of AZC systems, reacting CNF (0.65 mmol g^{-1} COO^-) with ethanolamine to obtain amidoethanol-functionalized CNF (CNF-CO-NH-CH_2-CH_2-OH, bearing ~ 0.3 mmol g^{-1} COO^-) results in an excellent increase in *G'* and *G''*. Only 0.1 % of CNFOH increases the *G'* and *G''* of metallogels by a factor of 5 and 6, respectively (orange symbols in **Fig. S10**). Moreover, increasing CNFOH content to 0.5 % (green symbols, **Fig. S10**), increases *G'* and *G"* by a factor of 20 and 40, respectively.

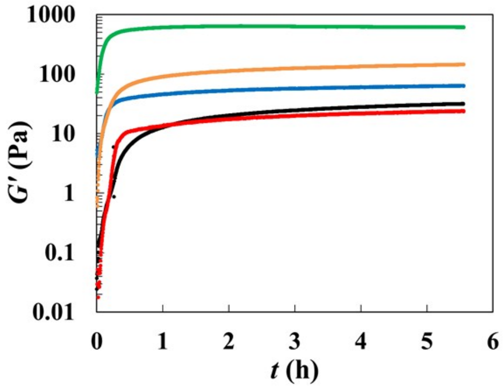

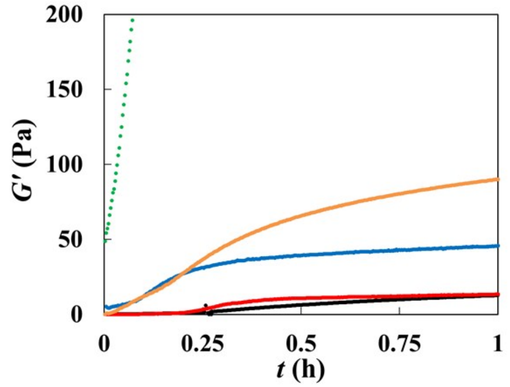

(a) Storage modulus *G'* versus time *t* at $\omega = 0.5$ rad s^{-1}, (upper panel) regular and (lower panel) zoomed-in graph.

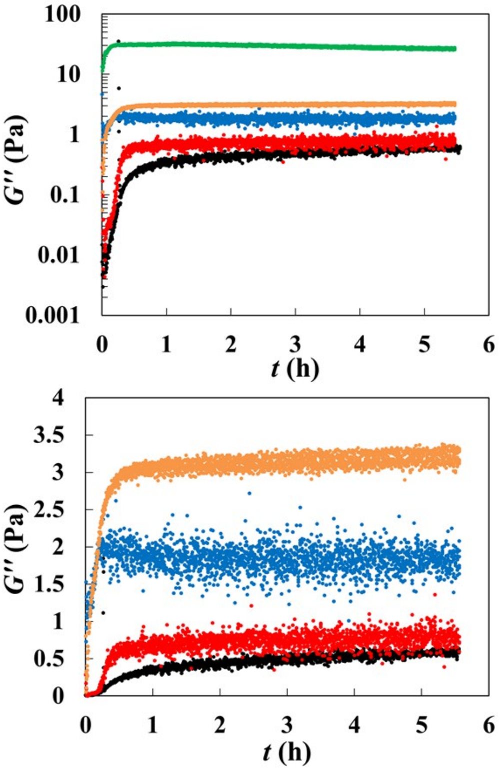

(b) Loss modulus *G''* versus time *t*, (upper panel) regular and (lower panel) zoomed-in graph.

Fig. S10: Viscoelastic evolution of AZC (0.5 %)-CNF nanocomposites at 80°C. Color legend is as follows: black (no additive), red (CNF 0.1 %), dark blue (CNF 0.5 %), orange (CNFOH 0.1 %), and green (CNFOH 0.5 %).

The gel formation rates of CNF nanocomposites are shown in **Fig. S11**. To obtain a significant increase in the gel formation rate, a high concentration of CNF is required; whereas, CNFOH is able to significantly accelerate the network formation and eliminate the induction time even at low concentrations, e.g., 0.1 %.

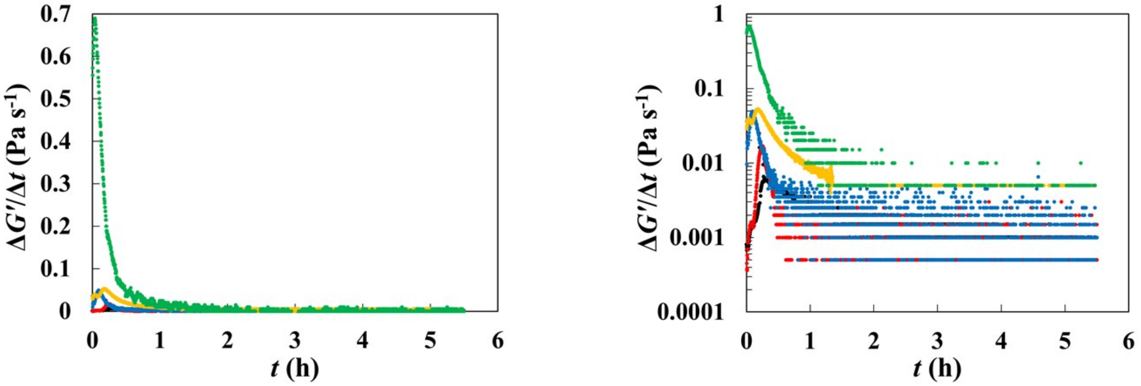

Fig. S11: Rate of storage modulus evolution versus time for CNF nanocomposites at 80°C and $\omega = 0.5$ rad s^{-1}, (left) regular and (right) semi-logarithmic scales. The color legend is the same as **Fig. S10**. Note that $\Delta t = 200$ s.

Figure S12 depicts the frequency response of CNF nanocomposites, which attests to their shear-thinning behavior even at a high crosslinking efficiency, achieved by CNFOH.

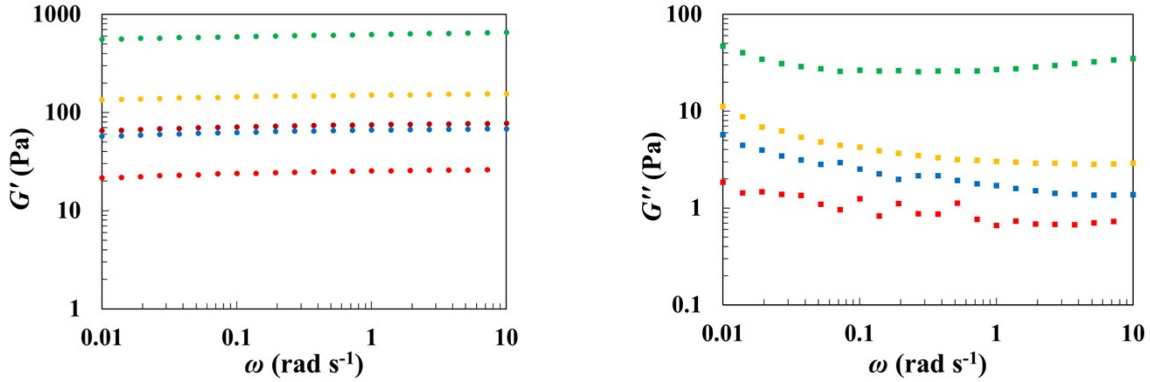

Fig. S12: Storage (left) and loss (right) moduli dependency of CNF nanocomposites on frequency, after gel formation at 80°C for 5.5 h. Color legend is the same as **Fig. S10**.

SNCC nanocomposites

While ENCC benefits from both steric and electrostatic interactions for colloidal stabilization, SNCC, bearing dialdehyde groups in the amorphous regions attached to the crystalline body, benefits only from the excluded volume of the dialdehyde cellulose chains. The repulsion achieved in this way is weaker than that of ENCC. **Figure S13** shows the viscoelasticity of AZC-SNCC nanocomposites. Similar to ENCC/DCC, the higher the concentration of SNCC, the lower are *G'* and *G''* due to the colloidal repulsion; however, at a desired concentration, the SNCC network strength (in terms of viscoelasticity) is higher than ENCC, which is in accordance with our proposed mechanism.

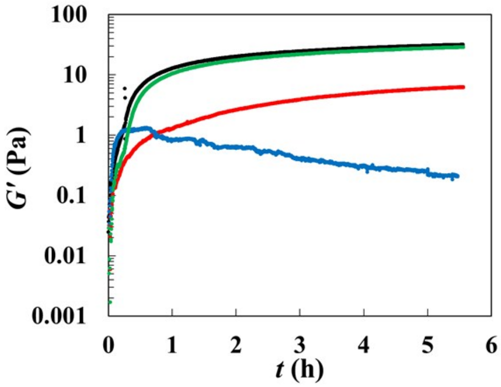

(a) Storage modulus *G'* versus time *t* at $\omega = 0.5$ rad s^{-1}.

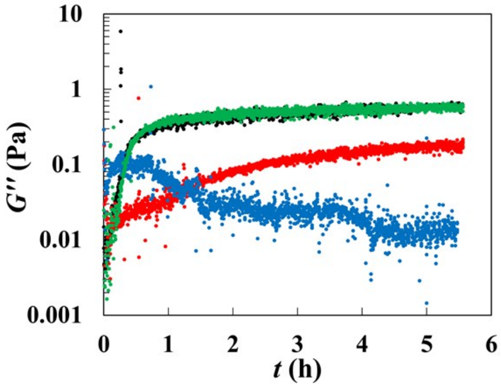

(b) Loss modulus *G''* versus time *t* at $\omega = 0.5$ rad s^{-1}.

Fig. S13: Viscoelastic evolution of AZC (0.5 %)-SNCC nanocomposites at 80°C. Color legend is as follows: black (no additive), green (SNCC 0.01 %), red (SNCC 0.1 %), and blue (SNCC 0.5 %).

Figure S14 presents gel formation rate versus time for the SNCC nanocomposites. Increasing SNCC concentration decreases the rate while the maximum rate is obtained faster.

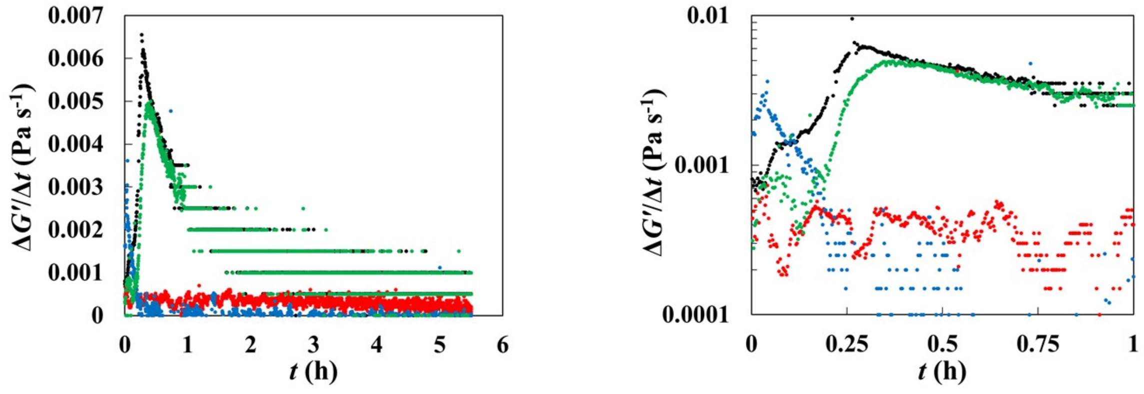

Fig. S14: Rate of storage modulus evolution versus time for SNCC nanocomposites at 80°C and $\omega = 0.5$ rad s^{-1}, (left) regular and (right) semi-logarithmic scales. The color legend is the same as **Fig. S13**. Note that $\Delta t = 200$ s.

Figure S15 shows the frequency response of SNCC nanocomposites. Similar to all AZC nanocomposites, SNCC-AZC composites exhibit a shear-thinning behavior.

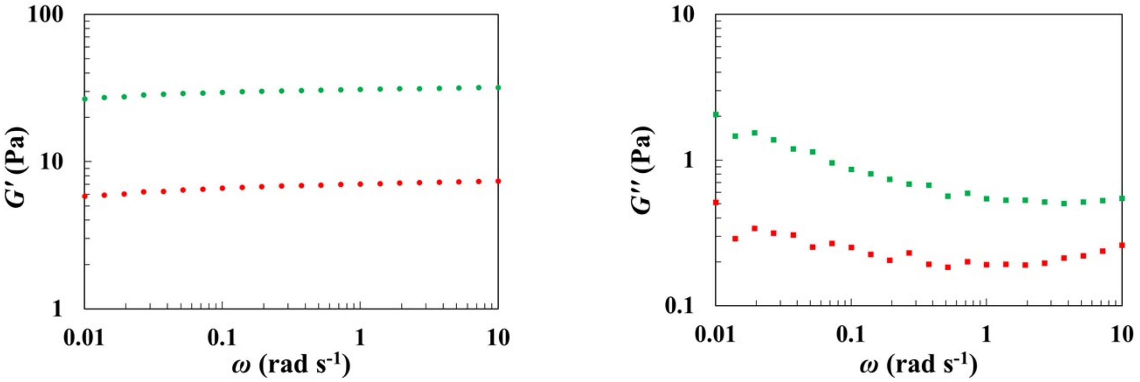

Fig. S15: Storage (left) and loss (right) moduli dependency of SNCC nanocomposites on frequency, after gel formation at 80°C for 5.5 h. Color legend is the same as **Fig. S13**. All samples have a shear thinning behavior. SNCC 0.5 % is not shown due to very low viscoelastic moduli.

The effects of nanocellulose-based colloidal toolbox on the rheological properties of AZC gels are summarized in Table S2.

Table S2. The effect of nanocellulose toolbox (0.5 wt %) on the storage modulus (*G'*), real part of the complex viscosity (η'), and activation time (t_i) of AZC (0.5 wt %) hydrogels undergoing crosslinking.

	Nanocellulose	G'/G'_0	η'/η'_0	$t_i/t_{i,0}$
Conventional	TEMPO-CNC	1.7	2.2	1.35
	CNC	2	3.4	0.65
	CNF	2	3.1	0.3
	CNFOH	20	42.7	0.15
Hairy	HENCC-2	6×10^{-1}	1.1	10
	HENCC-1	1.9×10^{-2}	3.4×10^{-2}	N/A
	ENCC	10^{-2}	6.6×10^{-3}	N/A
	SNCC	7×10^{-3}	1.9×10^{-2}	N/A
	DCC*	10^{-5}	10^{-3}	N/A

*Note: the viscoelasticity of AZC gels are obtained from small amplitude oscillatory shear (SAOS) rheometry of AZC gels undergoing crosslinking at 80ºC for 5.5 h. Subscript "0" denotes the additive-free AZC system. Here, $G'_0 \sim 30$ Pa, $\eta'_0 \sim 1.1$ Pa s, and $t_{i,0} \sim 1000$ s. *DCC concentration is 0.1 wt %. The weakened hairy nanocellulose-AZC gels may not exhibit a clear activation (induction) period in their rheological signature, hence, labeled as N/A.

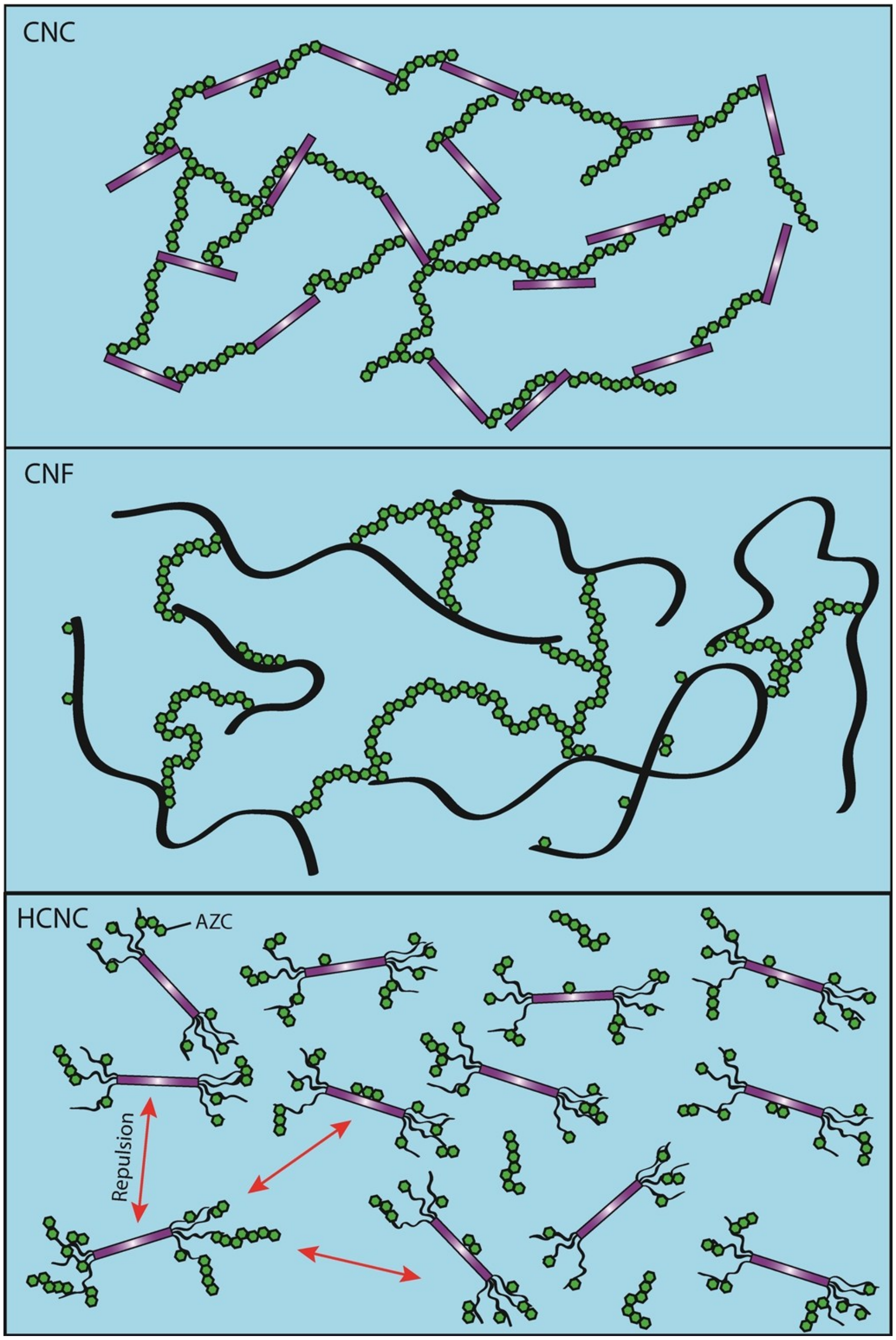

Scheme S1. Proposed mechanisms of nanocellulose-zirconium carbonate (ZC) interactions. Conventional cellulose nanocrystals (CNCs), bearing a low surface charge, integrate in and strengthen the ZC-ZC network. Similar to CNCs, cellulose nanofibrils (CNFs) are not affected by the colloidal repulsion and promote the macromolecular network formation. Hairy cellulose nanocrystals (HCNCs) bind to ZC and prevent ZC-ZC crosslinking in the bulk, as a result of electrosteric or steric repulsion. Tuning the colloidal properties of the nanocelluloses, the viscoelasticity of the metallogel nanocomposites may be precisely engineered. Note that these hypothetical mechanisms may warrant direct imaging/spectroscopy methods.

References

1 S. Safari, A. Sheikhi and T. G. M. van de Ven, *J. Colloid Interface Sci.*, 2014, **432**, 151–157.

2 T. G. M. van de Ven and A. Sheikhi, *Nanoscale*, 2016, **8**, 15101–15114.

3 A. Sheikhi and T. G. M. van de Ven, *Curr. Opin. Colloid Interface Sci.*, 2017, **29**, 21–31.

4 A. Sheikhi, S. Safari, H. Yang and T. G. M. van de Ven, *ACS Appl. Mater. Interfaces.*, 2015, **7**, 11301–11308.

5 L. Jowkarderis and T. G. M. van de Ven, *Cellulose*, 2014, **21**, 2511–2517.

6 H. Yang, A. Tejado, N. Alam, M. Antal and T. G. M. van de Ven, *Langmuir*, 2012, **28**, 7834–7842.

7 H. Yang, M. N. Alam and T. G. M. van de Ven, *Cellulose*, 2013, **20**, 1865–1875.

8 A. Sheikhi, H. Yang, M. N. Alam and T. G. M. van de Ven, *J. Vis. Exp.*, 2016, **113**, e54133.

9 H. Yang, D. Chen and T. G. M. van de Ven, *Cellulose.*, 2015, **22**, 1743–1752.

10 J. Araki, M. Wada and S. Kuga, *Cellulose.*, 2001, **17**, 21–27.